forum acusticum 2026
8-12 September · Graz, Austria

SLOW-SOUND OPTIMIZATION OF RAINBOW TRAPPING SILENCERS

Teresa Bravo[1], Cédric Maury[2], Daniel Mazzoni[3], Cédric Pinhède[2]

[1] *Spanish National Research Council (CSIC), Madrid, Spain*

[2] *Laboratory of Mechanics and Acoustics (LMA CNRS UMR 7031), Marseille, France*

[3] *Institute of Research on Non-Equilibrium Phenomena (IRPHE CNRS UMR 7342), Marseille, France*

This paper is a revised version of the authors' submitted manuscript that was peer-reviewed by at least two anonymous reviewers.

Abstract

Designing new kind of absorbers to avoid the use of porous or fibrous materials due to the presence of mean flow in a duct is a challenging topic in the field of noise control. Acoustic Black Holes (ABHs) have been derived with closed-ended configurations to achieve broadband absorption. These solutions are appropriate as anechoic termination but they cannot be used as silencers as they should allow the passage of the flow going through the axis of the duct. The use of open ABHs, also known as Rainbow-Trapping Silencers (RTSs) has been proposed to tackle this issue. RTSs are fully-opened in-duct metamaterials, of rectangular or cylindrical cross-sections, traversed by a low-speed flow and whose walls are lined by graded cavity depths. In order to reduce reflection and transmission and to obtain full dissipation of the acoustic disturbance over a broad bandwidth, a strategy is to enhance its slow sound properties. Parametric and optimization studies from theoretical (transfer matrix method) and numerical (finite element model) approaches show how a suitable choice of converging RTS parameters maximize slow sound effects. Such compact lightweight devices could be used to reduce broadband sound emissions in transport systems.

Keywords: *rainbow trapping filters, sound dissipation, slow-sound, transfer matrix*

1. Introduction

Noise dissipation within the low frequency band remains a subject of research due to limitations of classical control systems with sizes comparables to the working wavelength [1].

This challenge is especially relevant in ducted systems, where conventional passive treatments such as porous liners covered with perforated facings or resistive screens are widely used but become ineffective at low frequencies [2]. In addition to their limited acoustic efficiency in this range, such treatments also introduce aerodynamic pressure losses along the duct walls [3].

Development of acoustic metamaterials has brought new strategies exploiting the effective properties of engineered internal geometries [4]. They have demonstrated strong potential for controlling low-frequency broadband noise using subwavelength structures. Designs based on arrays of embedded Helmholtz resonators [5, 6], coiled channels [7], microperforations [8], skewed metaslits [9] and Fano resonances [10] have contributed to broadening the control bandwidth.

One of the mechanisms used to control wave propagation in acoustic metamaterials is the slow-sound effect. The effective velocity of acoustic waves decreases significantly within a region where the geometric properties of the resonant cells vary progressively to create strong dispersion [11]. As the wave propagates through such a region, its phase velocity gradually decreases, which can lead to enhanced energy trapping and dissipation.

A conceptual example of this effect occurs in a converging wave propagation domain that ends with a vanishing termination. This principle has previously been explored in the field of structural vibration control, particularly in thin beams and plates [12, 13]. It has been extrapolated as a serial distribution of quarter-wave resonators connected to a waveguide, referred as Acoustic Black Hole (ABH). These devices have been originally implemented as closed-ended configurations designed to achieve short anechoic terminations [14], acoustic wave focusing [15] or enhanced acoustic monitoring [16]. They consist of a sequence of rigid rings with gradually decreasing inner radii to produce a progressive reduction in acoustic wave speed as the wave approaches the termination,

Corresponding author: *teresa.bravo@csic.es.*

leading to near-complete wave trapping with minimal back-reflection. The mechanism results from the combined effects of cross-sectional variation and surface impedance changes at the cavity mouths [17, 18]. It has been argued that such rib-designed devices act essentially as Rainbow Trapping Silencers (RTS) [15], using graded, locally resonant structures that confine and trap the excitation wave at specific frequency-dependent locations.

When considering ventilated systems, open-ended ABHs have also been proposed for the simultaneous reduction of reflection and transmission by dissipating the incident energy inside the muffler [19]. It has been shown that widely-opened rib-designed mufflers, with an inlet-outlet radius ratio equal to one and axially increasing cavity depths, are retarding structures able to achieve near-unit dissipation over a broad bandwidth due to merging between the activated resonant cavities [20]. Geometric variations such as quadratic external flares have been found to extend the effective absorption bandwidth of converging RTSs toward lower frequencies compared with linear designs [21]. Most of the previous works have investigated the optimization of metaliners acoustic performance and less attention has been paid to the understanding of the slow-sound phenomena. Recently, Zhang *et al.* [22] have shown how sound speed decreases inside discrete ABH geometries, revealing the spatial distribution of wave deceleration during propagation. Experimental measurements using impedance tubes and movable MEMS microphones have explored the evolution of the wavefront propagation along the duct, and confirmed the slow-sound effect, demonstrating that acoustic waves can take approximately twice as long to propagate through an ABH structure compared with a rigid duct. Optimisation approaches have included studies on truncated ABHs by removing the shortest resonators [23] or the addition of perforation-modulated ABHs, where boundary perforation parameters significantly influence slow-sound enhancement [24].

The present study addresses the challenge of designing compact duct treatments that simultaneously reduce sound reflection and transmission over a wide frequency range while remaining compatible with airflow, by exploring the potential of slow-sound acoustic metamaterials. The authors propose a converging RTS, inspired by the convergent sections of low-speed wind tunnels, with the main objective of examining the slow sound effects while maintaining broadband acoustic efficiency. Sect. 2 presents an analytical transfer matrix formulation [14] for the prediction of the acoustic performance of the RTSs considering also the converging type silencer. A comparison with FEM results for model validation is included in Sect. 3. Conditions for slow-sound inside converging and straight RTSs are investigated for different frequency ranges and optimized geometries. We will finish with the main conclusions and ideas for future research work.

2. Theoretical description of Rainbow Trapping Silencers

The physical configuration considered is sketched in Fig. 1. It consists of an open RTS of total length $L = 0.15\ m$ along the z-axis, distributed among $N = 70$ cavities of width $d = 1.1$ mm, separated by walls of thickness $d_t = 3$ mm. The cavity depths $D(z)$ increase progressively accordingly to the law $D(z) = R[1 - \varphi_m(z)]$, with $\varphi_m(z) = (-z/L)^m$ and $m = 2.4$.

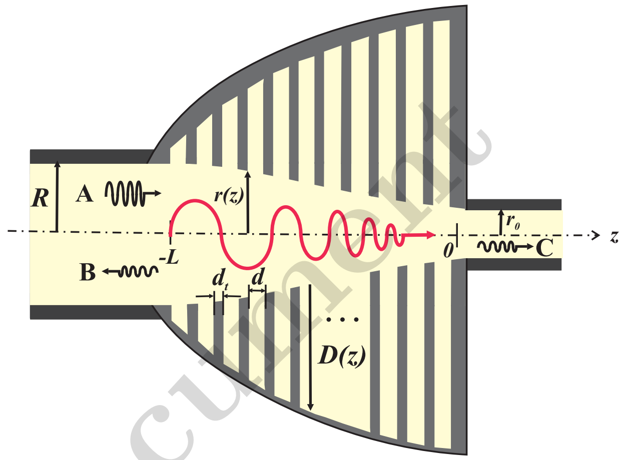

Figure 1. Schema of the physical set-up considered.

In order to achieve flow uniformity, the variation of the cross-section along the RTS axis follows a profile typically used in the design of low-speed wind tunnel convergent given by a fifth-order polynomial shape function for the inner radius, as follows

$$r(z) = R\left[1 + (1 - \kappa_0^{-1})\left(-6z'^5 + 15z'^4 - 10z'^3\right)\right], (1)$$

with $z' = 1 + z/L$, and κ_0 the contraction factor of the convergent nozzle, that has been optimised to take a value $\kappa_0 = 0.25$ [20]. The inlet and outlet radii are given respectively by $R = 0.04$ m and $r_0 = 0.01$ m. This profile is valid for inlet test section area smaller than $0.5\ \mathrm{m}^2$ and low-speed flows with a mean velocity lower than $40\ \mathrm{m \cdot s^{-1}}$. The optimal RTS parameters and convergent profile have been selected as a compromise between maximum acoustic performance and minimum drag forces influenced by the wall porosity and the contraction ratio [20].

2.1 Acoustic performance of RTSs

Analytical expressions have been obtained for the quantification of the sound propagation along a RTS presenting a convergent cross-sectional surface [21]. From the equation of propagation with varying wall admittance, assuming an infinite number of cavities and a low-frequency approximation, one obtains the axial phase speed $c_z' = \mathrm{Real}(c_z)$ given by

$$c_z' \approx \frac{c_0}{\kappa(z)(2 - \varphi_m(z))}, (2)$$

with c_0 the sound speed and $\kappa(z) = R/r(z)$ the local contraction ratio. Eq. (2), valid when $f \ll$

$c_0/(4\pi R) \approx 600$ Hz, shows how slow sound properties inside the RTS are enhanced at low frequencies due to the converging profiled silencer.

To evaluate how the contracting area affects the acoustic performance of the silencer, the Transfer Matrix Method (TMM) [14] can be used when considering plane wave propagation conditions and a discretised number of N cavity-wall units as indicated in Fig. 1. Applying continuity of the flow rate and pressure across the i^{th} cavity-rib cell, we can obtain the relation $[p_i\ u_i]^{\mathrm{T}} = \mathbf{T}_i\, [p_{i+1}\ u_{i+1}]^{\mathrm{T}}$, with $\mathbf{T}_i$ the individual transfer matrix defined as

$$\mathbf{T}_i = \begin{bmatrix} \cos[k_0(d+d_t)] & \mathrm{j}\dfrac{Z_0}{S_i}\sin[k_0(d+d_t)] \\ \mathrm{j}\dfrac{S_i}{Z_0}\sin[k_0(d+d_t)] & \cos[k_0(d+d_t)] \end{bmatrix} \times \begin{bmatrix} 1 & 0 \\ Y_{\mathrm{cav},i} & 1 \end{bmatrix}, (3)$$

where $k_0 = \omega/c_0$, ω the angular frequency, Z_0 the characteristic impedance of the air and $S_i = \pi r_i^2(z)$ the inner cross section. The total transfer matrix is obtained as the contribution of the individual cells, $\mathbf{T} = \prod_{i=1}^{N} \mathbf{T}_i$. The elements T_{ij} of this transfer matrix can be used to calculated the amplitudes of the reflections and transmission coefficients assuming a perfect anechoic downstream condition as

$$\begin{cases} 1 + r' = T_{11}t' + \dfrac{S_0}{Z_0}T_{12}t' \\ 1 - r' = \dfrac{Z_0}{S_R}T_{21}t' + \dfrac{S_0}{S_R}T_{22}t' \end{cases}, (4)$$

with $S_0 = \pi r_0^2$, and $S_R = \pi R^2$. The dissipation is then calculated as $\eta = 1 - |r'|^2 - |t'|^2 = 1 - \rho - \tau$ with ρ and τ the reflection and transmission coefficients.

2.2 Slow sound in RTSs

To quantify the slow-sound effect on the acoustic wave due to the convergent RTS a methodology has been developed. An array of probes equally spaced along the duct axis at positions $\{z_j\}$, $j = 1, \dots, J$ allows to acquire the real acoustic pressures at time steps $\{t_n\}$, $n = 1, \dots, N'$. The recorded time-domain signals are discrete Fourier-transformed at the probes positions at time intervals $\Delta t = t_{n+1} - t_n$ to provide $P(z_j; \omega)$. The probes are then grouped in pairs to calculate a two-probe decomposition to extract the forward travelling component $P^{+}(z_j; \omega)$ from the total Fourier-transform of the pressure. The progressive component of the complex pressure field at the axial position z_j and angular frequency ω can be written as

$$P^{+}(z_j; \omega) = \frac{P(z_{j-1}; \omega)\mathrm{e}^{\mathrm{j}k_0\,\Delta z_j} - P(z_j; \omega)}{\mathrm{e}^{\mathrm{j}k_0\,\Delta z_j} - \mathrm{e}^{-\mathrm{j}k_0\,\Delta z_j}}\mathrm{e}^{\mathrm{j}k_0\,z_j}, (5)$$

with $2 \leq j \leq J-1$ and Δz_j the separation distance between two probes to enable proper phase resolution. Using the frequency-domain TMM formulation, the forward component $P^{+}(z_j; \omega)$ can be expressed as $P^{+}(z_j; \omega) = |P^{+}(z_j; \omega)|\mathrm{e}^{-\mathrm{j}\phi(z_j;\omega)}$ with $\phi(z_j; \omega) = \arg[P^{+}(z_j; \omega)] \in]-\pi; \pi]$ the wrapped phase. $\varphi(z_j; \omega)$ can be calculated when this signal is unwrapped to obtain a continuous distribution avoiding the 2π jumps. The local axial wavenumber $k_z(z_j; \omega)$ is calculated taking the spatial derivative of the unwrapped phase as

$$k_z(z_j; \omega) = -\left.\frac{\mathrm{d}\varphi(z; \omega)}{dz}\right|_{z=z_j} (6)$$

Eq, (6) is calculated numerically defining a sliding spatial window with center at each z_j position and using a half-width window w with a linear regression of $\varphi(z_j; \omega)$ on the data points included within w. The axial phase velocity is then calculated as $c_z(z_j; \omega) = \omega/k_z(z_j; \omega)$. The procedure is performed at each frequency with a harmonic excitation and over a sliding spatial window scanning all the z-axis probe positions. We can also estimate the wave-front propagation time from spatial integration of c_z^{-1} at the probe positions when the excitation is propagating downstream the duct.

3. Simulated results

3.1 Acoustic performance

The acoustic performance of the convergent RTS has been calculated using the TMM formulation outlined in Sect. 2.1. The JCAL model of visco-thermal losses inside the cavities has been used [25]. Validation of the model is made against a set of numerical FEM simulations using the Thermoviscous Acoustics model implemented in Comsol Multiphysics in the frequency domain. It considers the viscous losses and the heat conduction in the fluid domain. The chosen mesh settings are such that the maximum element size was set to $d/3$, thereby ensuring at least ten nodal points per acoustic wavelength at the first duct cut-on frequency $f_c \approx 1.84\, c_0/(2\pi R)$ (the highest frequency of interest). The minimum element size was chosen as $\delta_v(\omega_c)/3$ ($\omega_c = 2\pi f_c$) in order to well resolve the visco-thermal boundary layers along the ABH rings and duct walls. Quadratic elements were used for the pressure, velocity and temperature fields considering a 2D axisymmetric geometry.

The reflection, transmission and dissipation spectra are represented up to 2.5 kHz in Figs. 2-4 respectively when estimated from both the analytical (plain) and numerical (dotted) approaches. A comparison has been included when considering the convergent RTS outlined in Fig. 1 and a constant cross-sectional RTS of radius $R = 0.04$ m associated to black and red colors respectively. The differences in the performance between both physical configurations can be clearly appreciated. The constant cross-section configuration provides low values for the reflection and transmission coefficient in a wideband starting at 1.5 kHz, whereas this low-frequency performance is displaced down to 750 Hz for the convergent RTS (C-RTS). The agreement between the TMM and FEM approaches is reasonably good, that validates the use of the TMM formulation for this particular configuration. The highest discrepancies appear for the C-RTS in the low frequency range, out of the efficiency frequency band.

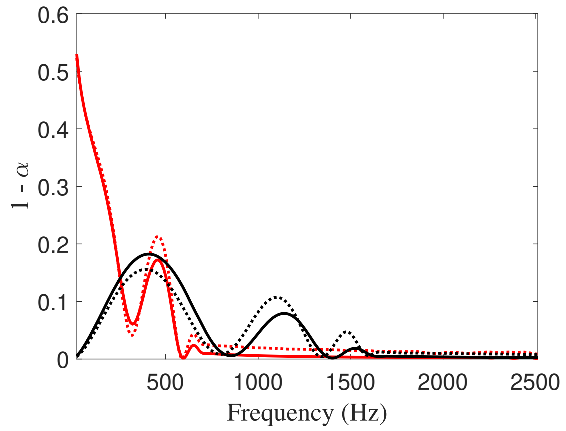

Figure 2. Reflection spectra of RTS (black) and C-RTS (red) from TMM (plain) and from FEM (dotted).

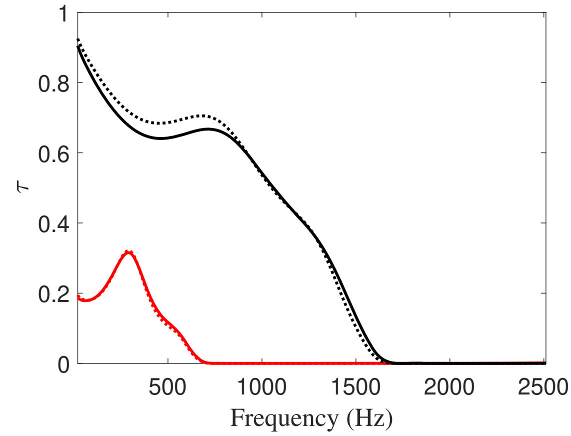

Figure 3. Transmission spectra of RTS (black) and C-RTS (red) from TMM (plain) and from FEM (dotted).

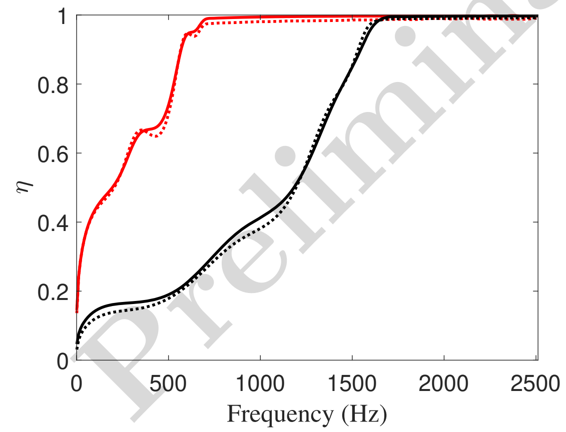

Figure 4. Dissipation spectra of RTS (black) and C-RTS (red) from TMM (plain) and from FEM (dotted).

One observes in Fig. 4 a maximum of dissipation for the C-RTS at 311 Hz (TMM) and 331 Hz (FEM) respectively, that does not appear for the straight RTS. It is due to the first axial half-wavelength resonance that satisfies zero-pressure condition at the inlet and outlet of the converging silencer. This resonance is activated at such low frequency because it scales with the mean phase speed, c_z, across the C-RTS rather than the sound speed c_0. This is due to the slow-sound effect (Eq. (2)) at low frequency, which becomes more important as the contraction ratio κ_0 increases.

3.2 Slow-sound along the waveguide

Propagation of the forward acoustic wavefront along the lined duct has been implemented using the TMM formulation according to Sect. 2. The axial phase velocities have been computed for five different frequencies from 300 Hz to 2 kHz. The results are superimposed in Fig. 5 for the classical RTS with constant cross-section as a function of the axial position, where the location of the silencer has been marked as the yellow area.

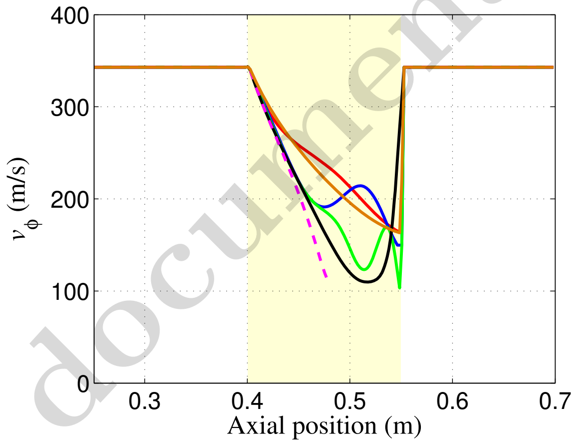

Figure 5. Axial variations of the phase velocity within a RTS (yellow area) estimated from TMM at 300 Hz (brown), 500 Hz (red), 1000 Hz (blue), 1500 Hz (green), 1700 Hz (black) and 2000 Hz (magenta dashed).

We can see that the axial phase speed starts to decrease progressively form the RTS inlet achieving minimum values close to the outlet. It should be noted that out of the RTS position, the average phase speed is estimated with a value of $344\ \mathrm{m.s^{-1}}$, close to the sound speed as expected. The minimum values achieved inside the RTS for the estimated phase speed are related with the value of the excitation frequency, getting smaller as we increase the frequency towards the band of maximum dissipation performance that starts at 1600 Hz. For these frequencies under 1600 Hz, a minimum phase speed is reached at the RTS outlet that stays well below $c_0/2$. Above 1600 Hz, the minimum phase speed is achieved at the location of the resonant cavities and its minimum value increases with frequency.
To compare the slow sound effects inside a classical RTS (Fig. 5) with those in the C-RTS, we have plotted the axial phase speed for the physical configuration with varying cross-section (Fig. 6). For clarity, the dashed curves in Figs. 5 and 6 have been presented only in the slow sound regime, *i.e.* up to the axial positions at which the phase speed reached its minimum value within the silencers. It can be seen that the minimum phase speed values achieved inside

the C-RTS extend over a wider bandwidth, here between 300 Hz and 700 Hz, with respect to the RTS case. Also, it reaches smaller values than in the RTS case as long as the excitation frequency stays below the respective ranges of high efficiency. Moreover, slow-sound variations inside the C-RTS are less-dependent on the excitation frequency than in the straight RTS. Indeed, the different phase speed curves in Fig. 6 show less variability than in Fig. 5.

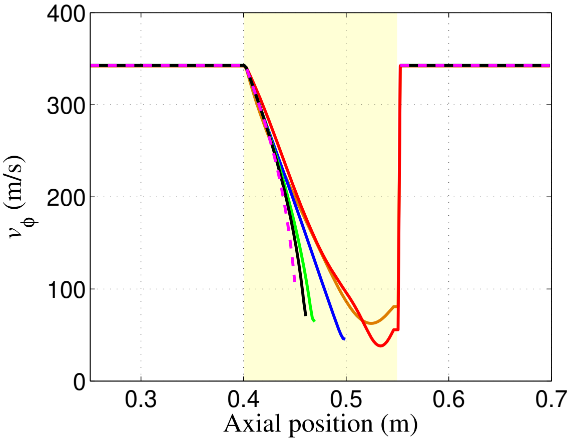

Figure 6. Axial variations of the phase velocity within a C-RTS (yellow area) estimated from TMM at 300 Hz (brown), 500 Hz (red), 1000 Hz (blue), 1500 Hz (green), 1700 Hz (black) and 2000 Hz (magenta dashed).

To better understand which factors enhance the slow-sound effect in C-RTSs, we have selected a set of four physical constituting parameters $(m, N, d, D_{\max})$. They have been varied with the objective of achieving the lowest value for the axial phase velocity. As this is multi-functional optimisation problem with a non-linear cost function, Particle Swarm algorithm [26] has been used to find the global minimum. This algorithm mimics the interactions of group species such as bird or fishes, progressively adapting the solutions with collective knowledge. To achieve slow-sound, the cost function to be minimized has been selected as the 2-norm of the phase velocity c_z over the length of the C-RTS, defined as $\|c_z\|_2 = \sqrt{\sum_{i=1}^{N} |c_z(z_i)|^2}$, z_i being the axial location of the i^{th} cavity-rib cell. The optimal parameters are $(m_{\text{opt}}, N_{\text{opt}}, d_{\text{opt}}, D_{\max,\text{opt}}) = (3, 30, 0.004\ \text{m}, 0.07\ \text{m})$, leading in Fig. 7 to a minimum phase speed of $c_0/11$ instead of $c_0/4$ when the total dissipation is maximized. This involves a decrease of the number of cavities, of their width and a steeper cavity profile, when compared to the optimal parameters that maximize the C-RTS dissipation performance.

4. Conclusions

In this work we have made a comparison between two different RTS configurations including a classical geometry with a constant inlet radius and a convergent configuration with varying cross-section. The analytical TMM validated against a FEM numerical model have confirmed the superior acoustic performance of the C-RTS in terms of the lowest bound for maximum dissipation over a broad frequency band.

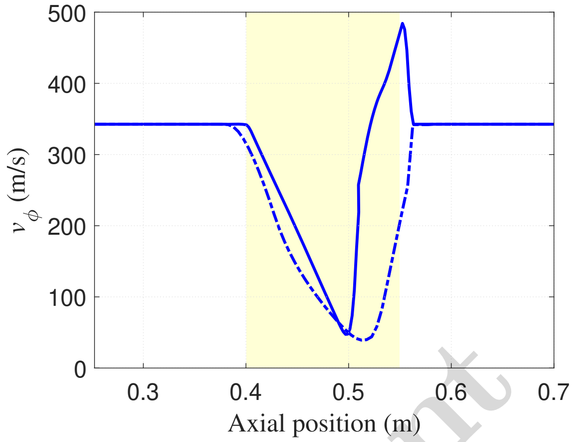

Figure 7. Axial variations of the phase velocity estimated from TMM at 1000 Hz within a C-RTS (yellow area) when the total dissipation is maximized (solid blue) and when the 2-norm of the phase velocity is minimized (dashed-dotted blue).

A formulation for characterizing the slow sound effect has been developed using the unwrapped phase of the pressure phase signal acquired by an array of probes along the axial coordinate. The C-RTS is able to achieve a minimum phase speed of $c_0/11 \approx 31.2\ \text{m.s}^{-1}$ compared to $c_0/4 \approx 85.7\ \text{m.s}^{-1}$ for the classical RTS. It constitutes a promising device to effectively increase the slow sound without increasing the material size.

5. Acknowledgments

This work is part of the project PID2022-139414OB-I00 funded by MCIN/AEI/10.13039/501100011033/ and by "ERDF A way of making Europe". It has also received support from the French government under the France 2030 investment plan, as part of the Initiative d'Excellence d'Aix-Marseille Université - A*MIDEX (AMX-22-RE-AB-157). We wish to thank the PSIVA platform of the Laboratoire de Mécanique et d'Acoustique for the use of its outstanding equipment.

References

[1] S. Huang, Y. Li, J. Zhu and D. P. Tsai: "Sound-Absorbing Materials," *Physical Review Applied*, vol.20, pp. 010501, 2023.

[2] T. Zhong, C. Yang and M. Åbom, "Tonal noise reduction of an electric ducted fan using over-the-rotor acoustic treatment," *Applied Acoustics,* vol. 205, pp. 109298, 2023.

[3] B. M. Howerton and M. G. Jones, "Acoustic Liner Drag, Measurements on Novel Facesheet Perforate Geometries," *in Proc. of the 22nd AIAA/CEAS Aeroacoustics Conference*, (Lyon, France), pp. 1-12, 2016.

[4] G. Fusaro, D. D'Orazio and M. Garai, "Review of metamaterials principles and methods in

ventilation ducts: 1928–2024," *Journal of the Acoustical Society of America*, vol. 158, pp. 4560–4581, 2025.

[5] Y. Li and Y. S. Choy, "Broadband and low-frequency sound absorption of compact meta-liner under grazing flow," *Applied Acoustics*, vol. 224, pp. 110146, 2024.

[6] S. Xu, X. Xiao, L. Li and Z. Wen, "Innovative compact low-frequency absorber design: Integrating power-law-varying aperture into Helmholtz resonator," *Journal of Applied Physics*, vol. 138, pp. 083104, 2025.

[7] L. Li, T. Chen, L. Zhao and C. Bi, "Enhanced far-field acoustic signal detection via a deep subwavelength Fabry-Pérot resonator coupled with space-coiling metamaterial," *Mechanical Systems and Signal Procesing*, vol. 244, pp. 113745, 2026.

[8] M.L. Fung, S.K. Tang and M. Leung, "Sound transmission across a rectangular duct section with a thin micro-perforated wall backed by a sidebranch cavity," *Applied Acoustics*, vol. 219, pp. 109920, 2024.

[9] H. Emoto and T. Yamada, "Acoustic metaslit for regional sound insulation for a three-dimensional diffuse sound field incidence," *Applied Acoustics*, vol. 228, pp. 110297, 2025.

[10] D.-K. Lin, X.-W. Xiao, C.-C. Yang, S.-Y. Ho, L.-C. Chou, C.-H. Chiang, J.-S. Chen and C.-H. Liu, "An acoustic impedance design method for tubular structures with broadband sound insulations and efficient air ventilation," *Applied Acoustics*, vol. 220, pp. 109983, 2024.

[11] N. Jiménez, V. Romero-García, V. Pagneux, V.and J.V. Groby, "Rainbow-trapping absorbers: Broadband, perfect and asymmetric sound absorption by subwavelength panels for transmission problems," *Scientific Reports*, vol. 7, pp.13595, 2017.

[12] M.A. Mironov and V.V. Pislyakov, "One Dimensional Acoustic Waves in Retarding Structures with Propagation Velocity to Zero," *Acoustical Physics*, vol. 48, pp. 347–352, 2002.

[13] B. M. P. Chong, L. B. Tan, K. M. Lim and H. P. Lee, "A review on Acoustic Black-Holes (ABH) and the experimental and numerical study of ABH-featured 3D printed beams," *International Journal of Applied Mechanics*, vol. 9, pp. 1750078, 2017.

[14] O. Guasch, M. Arnela and P. Sánchez-Martín, "Transfer matrices to characterize linear and quadratic acoustic black holes in duct terminations," *Journal of Sound and Vibration*, vol. 395, pp.65–79, 2017.

[15] A. Mousavi, M. Berggren, L. Hägg and E. Wadbro, "Topology optimization of a waveguide acoustic black hole for enhanced wave focusing," *Journal of the Acoustical Society of America*, vol. 155, pp. 742–756, 2024.

[16] Zuanbo Zhou, Niaoqing Hu, Yi Yang, Zhengyang Yin, Jiangtao Hu and Xiaosong Lin, "Sonic black hole based metamaterial structure for contactless rotating machinery state sensing enhancement," *Measurement*, vol. 259, Part A, pp. 119613, 2026.

[17] G. Serra, O. Guasch, M. Arnella, D. Miralles, Optimization of the profile and distribution of absorption material in sonic black holes, "*Mechanical Systems and Signal Processing*", vol. 202, pp. 110707, 2023.

[18] A. Mousavi, M. Berggren and E. Wadbro, "How the waveguide acoustic black hole works: A study of possible damping mechanisms," *Journal of the Acoustical Society of America*, vol. 151, pp. 4279–4290, 2022.

[19] Y. Mi, W. Zhai, L. Cheng, C. Xi and X. Yu, "Wave trapping by acoustic black hole: Simultaneous reduction of sound reflection and transmission," *Applied Physics Letters*, vol. 118, pp. 114101, 2021.

[20] T. Bravo and C. Maury, "Broadband sound attenuation and absorption by duct silencers based on the acoustic black hole effect: Simulations and experiments," *Journal of Sound and Vibration*, vol. 561, pp. 117825, 2023.

[21] T. Bravo and C. Maury, "Converging rainbow trapping silencers for broadband sound dissipation in a low-speed ducted flow," *Journal of Sound and Vibration*, vol. 589, pp. 118524, 2024.

[22] X. Zhang, N. He, L. Cheng, X. Yu, L. Zhang and F. Hu, "Sound absorption in sonic black holes: Wave retarding effect with broadband cavity resonance," *Applied Acoustics*, vol. 221, pp. 110007, 2024.

[23] Y.-H. Yu, W. Huang, L.-X. Xie, Z.-H. Li, X. Li and M.-H. Lu, "Broadband sound absorption and slow wave in truncated sonic black hole," *Applied Acoustics*, vol. 235, pp. 110677, 2025.

[24] S. Li, X. Yu and L. Cheng, "Enhancing wave retarding and sound absorption performances in perforation-modulated sonic black hole structures", *Journal of Sound and Vibration*, vol. 596, pp. 118765, 2025.

[25] D. L. Johnson, J. Koplik and R. Dashen, "Theory of dynamic permeability and tortuosity in fluid-saturated porous media", *Journal of Fluid Mechanics* vol. 176, pp. 379–402, 1987.

[26] J. Kennedy and R. Eberhart, "Particle swarm optimization", *in Proc. of the IEEE International Conference on Neural Networks, Vol. 4*, (Perth, Australia), pp. 1942–1948, 1995.